Nanoscale

Volume 1 | Number 1 | Jan 2013 | Pages 1–100

Nanoscale

www.rsc.org/nanoscale

ROYAL SOCIETY
OF CHEMISTRY

ROYAL SOCIETY
OF CHEMISTRY

www.rsc.org/nanoscale

Journal Name

ARTICLE

Toward highly radiative white light emitting nanostructures: a new approach for dislocation-eliminated GaN/InGaN core-shell nanostructures with a negligible polarization field

Je-Hyung Kim, Young-Ho Ko, Jong-Hoi Cho, Su-Hyun Gong, Suk-Min Ko, and Yong-Hoon Cho*

White light emitting InGaN nanostructures hold a key position in the future solid-state lighting applications. Although many suggestive approaches to form group III-nitride vertical structures have been reported, more practical and cost effective methods are still needed. Here, we present a new approach for GaN/InGaN core-shell nanostructures on a wafer level formed by chemical vapor-phase etching and metal-organic chemical vapor deposition. Without a patterning process, we successfully obtained high quality and polarization field minimized In-rich GaN/InGaN core-shell nanostructures. The various quantum well thicknesses and the multi-facets of the obelisk-shaped core-shell nanostructures provide a broad spectrum of the entire visible range without changing the InGaN growth temperature. Due to their high crystal quality and polarization field reduction, the core-shell InGaN quantum wells show an ultrafast radiative recombination time less than 200 ps and uniformly high internal quantum efficiency in the broad spectral range. We also investigated the important role of polarization fields in the complex recombination dynamics in InGaN quantum wells.

Introduction

Semiconductor based solid-state lighting have high efficiency, high stability, fast response time, minimized size, and color tunability.[1-3] Therefore, they are currently replacing existing lighting and display systems that rely on bulbs or lamps. InGaN quantum well (QW) based wide bandgap semiconductors are leading this evolution with their broad spectral coverage and high quantum efficiency. However, the commercialized white light emitting diodes (LEDs), the most important lighting applications, are based on blue emitting InGaN QWs mixed with yellow emitting phosphors. The use of phosphors possesses many disadvantages, such as color conversion loss, a low color rendering index, a low modulation speed, and the increasing cost of phosphors.[4] Therefore, the development of phosphor-free white light emitting devices is greatly needed. The main obstacle of InGaN QW based phosphor-free white LEDs is a low quantum efficiency in long wavelength regions such as green and red.[5] Although the group III-nitride systems, can

theoretically cover the entire visible range by controlling the In composition, a large In content in InGaN QWs induces lots of strain that yields strong built-in electric fields and dislocations.[6, 7] This causes weak radiative and strong nonradiative recombinations of excitons in long wavelength region. Another problem of the conventional InGaN QWs grown on c-plane substrates is the limitation of QW thickness. As the QW thickness increases, the increased strain forms dislocations, and the quantum confined Stark effect (QCSE) becomes radically enhanced in the InGaN QWs. Therefore, thin QWs with a thickness of 2~3 nm are mostly used for LED applications. However, the use of thin QWs becomes one reason for a severe efficiency droop at a high carrier density.[8, 9] Furthermore the limited light extraction efficiency in a planar structure should be improved.

Several approaches have been suggested to obtain bright and broad emission from InGaN QWs. For example, the adoption of photonic crystal patterns,[10] a patterned substrate,[11] or surface texturing[12] have shown an increase in light extraction. The lateral overgrowth techniques[13] have been popularly used to improve the

crystal quality. The quaternary AlInGaN layer[14] or InGaN QWs grown on semipolar or nonpolar substrates[15] have also been suggested to reduce the polarization fields.

However, in many points of view, GaN/InGaN core-shell structures[16-19] are a promising approach for high efficiency light emitting devices since they can solve the above problems simultaneously. We can expect improvement in light extraction, reduction in dislocations, and relaxation in strains by introducing nanostructures. Furthermore, GaN/InGaN core-shell structures can effectively reduce the built-in electric fields by growing InGaN QWs on semipolar or nonpolar facets.[20] They also have a large emitting surface area, which increases the light output power and decreases the current density

For these reasons, many groups have concentrated their efforts in forming vertical GaN nanostructures. At an early stage, molecular beam epitaxy (MBE) techniques were used to grow vertical GaN nanostructures on Si substrates, where a disk type of InGaN QW was inserted (axial type).[21, 22] Recently, some groups successfully demonstrated metal-organic chemical vapor deposition (MOCVD) grown vertical GaN nanostructures by using catalysis,[23] patterning processes,[17, 24] or self-organized methods with a Si dopant.[25-27] Although extensive studies have been done, the formation of high-quality, high-density, vertical GaN nanostructures still has many limitations based on their approaches.

In this Letter, we introduce a fascinating method to form highly radiative, broad spectrum emitting GaN/InGaN core-shell nanostructures by using chemical vapor-phase etching (CVE) and MOCVD. Our approach is a hybrid method combining chemical top-down and bottom-up processes and it has many advantages. For example, without patterning work, it forms high crystal quality, vertical GaN nanostructures on a wafer scale by eliminating dislocations. The formed core-shell InGaN QWs show distinctive optical properties compared to the conventional planar InGaN QWs grown on a *c*-plane sapphire substrate. Together with an improved light extraction, the enhanced crystal quality, the strain relaxation, and the minimized polarization field in core-shell nanostructures induce highly radiative QW emission in a broad spectral range. We also observed the formation of In-rich InGaN QWs with various QW thicknesses in core-shell nanostructures, which is limited in planar QWs.

Results and discussion

Formation of GaN/InGaN core-shell nanostructures

It is well known that the conventional physical etching induces severe etching damage, and there is no proper chemical wet etchant for GaN due to the strong mechanical and chemical strength of GaN materials.[28, 29] However, with the CVE method, self-formed, high crystal quality nanostructures can be obtained by dislocation- and facet-selective etching mechanisms. First of all, to obtain high quality nanostructure templates, we exposed a GaN thin film to HCl gas at a high temperature around 1000 °C. In our etching experiments, HCl effectively decomposes GaN into GaCl (GaN + HCl → GaCl + 1/2H$_2$ + 1/2N$_2$), and this etching action becomes negligible below 800 °C. Due to the nature of chemical reaction of the CVE process, the size and shape of etched nanostructures can be modified by controlling the etching conditions such as temperature, time, and HCl flow. During the etching process, dislocations are etched first, and therefore the formed nanostructures have high crystal quality and reduced strain. Details on the CVE method and the improved structural and optical characteristics in as-etched GaN nanostructures have been reported elsewhere.[30]
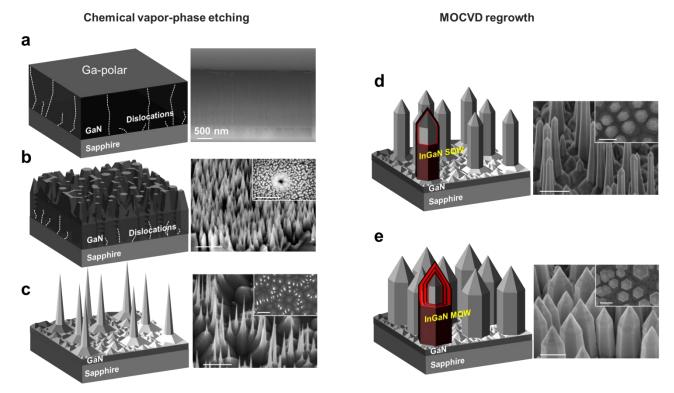

Fig. 1 (a-e) Schematics and tiled-view SEM images for (a) 2 *μ*m-thick GaN film on 2-inch sapphire substrates, (b) early stage of CVE etching, (c) as-etched vertical GaN nanostructures by CVE process, (d,e) MOCVD regrown GaN/InGaN core-shell nanostructures including (d) SQW and (e) MQWs. Insets: top-view SEM images. Scale bars = 500 nm
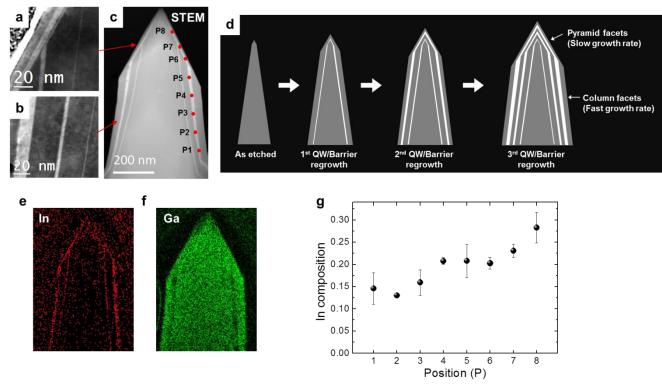
Fig. 2 (a,b) Cross-sectional scanning TEM high-angle annular dark field image of (c) core-shell MQWs and high magnification images at (a) pyramid facet and (b) column facet. (d) Schematic representation for the growth of core-shell MQWs. (e-f) Element mapping images for (e) In and (f) Ga atoms by using EDS. (g) In composition plot from the core-shell InGaN MQWs at various positions. The measured points are marked in (c).

Based on the etched GaN nanostructure templates, we regrew InGaN QWs and GaN barriers by using MOCVD to form GaN/InGaN core-shell nanostructures. Fig. 1a-e shows schematic representations and SEM images at each step of CVE and MOCVD regrowth process for GaN/InGaN core-shell nanostructures. At an early stage of CVE process (Fig. 1b), the thin GaN film starts to change the surface morphology, and the dislocations are rapidly eliminated by forming the hexagonal etched pits due to their weak crystal quality (inset in Fig. 1b). After then, the tapered vertical GaN nanostructures are formed as a result of CVE process (Fig. 1c). During the MOCVD regrowth process, lateral growth more likely occurs than axial growth, resulting in hexagonal faceted, obelisk-shaped GaN/InGaN core-shell nanostructures, which consist of a vertical column part and a pyramidal tip part. We made two samples including single QW (SQW) and three-periods, multiple QWs (MQWs), respectively (Fig. 1d and 1e). They have average height and density about 1 μm and 6 x 10^8/cm^2, respectively.

To confirm the formation of InGaN QWs, we performed transmission electron microscopy (TEM) measurement. Fig. 2a-c show the cross-sectional TEM images of GaN/InGaN core-shell MQWs. We also fabricated conventional planar MQWs grown on a 2-μm thick GaN film as references (See Fig. S1† for more TEM images of the core-shell and the planar QWs). Both the core-shell and the planar QWs were grown simultaneously at the same growth conditions for comparison. In the case of SQW, the QW growth time and temperature were 100 s and 680 °C, respectively. For MQWs, we grew three periods QWs with growth times of 100 s, 300 s, and 900 s and growth temperature of 680 °C in order to study the influence of the QW thickness. All other growth conditions were identical.

In TEM images, the GaN/InGaN core-shell nanostructures do not show any dislocations inside and have very clean surfaces, which are important advantages of the CVE process. In the case of planar structures, it was quite difficult to grow a high-quality, thick InGaN QW with high In contents due to the accumulated large strain (Fig. S1d†). The critical thickness of planar InGaN QWs is known to be less than 10 nm with high indium contents around 20 ~ 30 %.[31] The TEM image in Fig. 2a also shows a large change in the QW growth rates between the vertical column part and the pyramidal tip part of core-shell nanostructures (See also Fig. S1c†). The column part has a faster growth rate more than twice compared to that of the pyramidal tip part. Due to the relatively slow growth rate of the pyramid facets, the area of pyramid facets becomes wider as the nanostructures grow (Fig. 2d).[32] The measured thickness of the core-shell QWs are summarized in Table 1. The QW growth rate also depends on the base templates: the planar QWs grown on a c-plane show two times faster growth rate compared to the core-shell QWs (Fig. S1†).

We note that a relatively low QW growth temperature was used to obtain high In contents in InGaN QWs for longer wavelength emission. The In composition of the core-shell InGaN QWs was measured by the energy dispersive X-ray spectroscopy (EDS). Fig. 2e and 2f show atomic compositional mapping images for In and Ga atoms, respectively, and Fig. 2g shows the position-dependent In composition change. The results show a large variation of In contents from 15 % to 30 % depending on the vertical position of nanostructures. The higher position of nanostructures we measured, the higher In composition we observed. This position-dependent composition variation originated from the different diffusion lengths of In and Ga adatoms.[33, 34] The above In variation was investigated from the third, thickest QW, and the second QW also showed the similar In compositions and trends. However, for the first, thinnest QW, it was difficult to extract the exact In composition values due to its narrow QW thickness less than 1 nm.

Table 1 Comparison of the thickness of SQW or MQWs grown on various facets

	SQW	Core-shell MQWs		
		1st	2nd	3rd
Growth Time (s)	100	100	300	900
Thickness at Column part (nm)	0.89±0.28	0.99±0.09	4.93±0.60	15.51±0.66
Thickness at Pyramid part	1~2 (monolayer)	1~2 (monolayer)	1.72±0.07 (nm)	8.15±0.82 (nm)

It is worth noting that high crystal quality, high In content InGaN QW can be formed with various thicknesses. A thick InGaN QW is an important structure for bright and high power photonic devices because the thick InGaN QWs can have less current density at a high input current level, which improves the efficiency droop.[9] In the case of a thin QW, we can expect high oscillator strength.[35] In addition, the possibility of high quality QWs with a wide thickness range in the core-shell structures enables to control the transition energy of InGaN QWs in a broader range via QW thickness. Both thick and ultrathin QWs are not easy to form in c-oriented planar structures using MOCVD, especially with a high In composition, since the enlarged strain occurs many dislocations in thick QWs to release strain[31], and the fast growth rate in the *c*-plane makes it more difficult to control the narrow thickness of QWs. Furthermore, we have also observed the formation of three-dimensionally confined quantum structures at the top apex of nanostructures, and the confined single quantum structures showed the possibility as efficient single photon sources.[36]

Broad photoluminescence (PL) emission from GaN/InGaN core-shell nanostructures

An improved crystal quality and a morphological change of the core-shell InGaN QWs have a strong influence on their optical properties. In Fig. 3, we compared low temperature (10 K) PL spectrum (log scale) of InGaN SQW and MQWs grown on etched nanostructures. Interestingly, the core-shell SQW and MQWs show a large difference in their emission wavelength. The PL spectrum of the core-shell SQW shows a blue emission, while the core-shell MQWs show a broad emission from blue to red. To explain the exciton transition energy of InGaN QWs, we considered various factors such as In composition, QW thickness (quantum confinement effect), and polarization field (quantum confined Stark effect
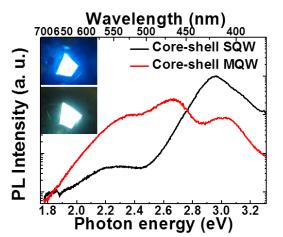

Fig. 3 Comparison of PL spectrum at 10 K for core-shell SQW (black line) and MQWs (red lines). Inset: photo images of the core-shell SQW (top: blue emission) and the core-shell MQW sample (bottom: cyanish white emission)

(QCSE)). As already shown in TEM images, the core-shell InGaN QWs are grown on various semipolar facets and have various QW thicknesses, leading to a reduction of built-in electric fields and a change of quantum confinement effect. The In composition of in core-shell nanostructures also depends on the vertical position. Among these factors, the quantum confinement effect is one of dominant reason for the blue emission in the core-shell SQW. The modification of exciton transition energy by the quantum confinement effect is less than 0.2 eV for the 1 nm thick QW.[37] However, if we consider the low growth temperature, and thus high In contents in InGaN QWs, the emission energy of the core-shell SQW has a larger blue shift than we expected from Fig. 2g. This indicates the thin InGaN SQW has lower In composition compared to the thick InGaN QWs, which measured in Fig. 2g. This limited In incorporation efficiency in a thin QW can be explained by the compositional pulling effect.[38] The reduced quantum confinement effect and improved In incorporation efficiency in a thick InGaN QW can be confirmed by the core-shell MQW sample including various QW thicknesses. In Fig. 3, the core-shell MQWs have a very broad PL spectrum compared to the core-shell SQW, and show distinctive three peaks. The PL emission at 2.98 eV in the core-shell MQWs originated from the first innermost, thinnest QW, which has similar QW thickness and emission wavelength to the core-shell SQW, and therefore, the low energy part of PL emission below 2.8 eV comes from the second and the third QWs in the core-shell MQW with reduced quantum confinement effect and increased In
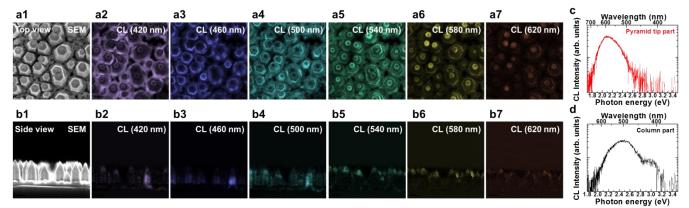

Fig. 4 (a1-b7) SEM images and monochromatic CL images at various wavelengths for the core-shell InGaN MQWs. (a1-a7) Top view and (b1-b7) side view. (c,d) Point CL spectrum measured at (c) pyramid tip part and (d) column part.

contents. In this low energy part of PL emission, there are two distinctive peaks at 2.7 eV and 2.35 eV. These two peaks are attributed to the InGaN emission from different positions, i.e., the pyramid tip and column regions. As shown in Fig. 2g, the pyramid tip has higher In content than the column part. We performed the cathodoluminescence (CL) experiments at room temperature to examine the emission property depending on the position of the nanostructures. Fig. 4a1-a7 (b1-b7) show SEM and monochromatic CL images at top (side) view and at various wavelengths. As expected, the pyramid tip of nanostructures emits longer wavelength than the column part. The point CL spectrum in Fig. 4c,d also show different emission wavelength between the pyramid and the column part, which reveal the origin of the second (2.7 eV) and the third (2.35 eV) peaks in Fig. 3. The CL data of core-shell SQW, showing an emission peak at 2.9 eV, can be shown in Supplementary Information (Fig. S2†). Therefore, together with various thicknesses of InGaN QWs, the large variation in In composition enables a broad spectrum without changing the InGaN growth temperature, resulting in cyanish white color emission (inset in Fig. 3, Fig. S3†). To confirm that the long wavelength emission around 2.3 eV is from the QW emission, not from the yellow luminescence in GaN,[39] we performed the PL excitation (PLE) experiment and observed a strong InGaN absorption signal, which is a strong evidence of InGaN QW emission (Fig. S4†).

Carrier recombination dynamics of GaN/InGaN core-shell nanostructures

A dramatic change between the core-shell and the planar InGaN QWs occurs in their recombination dynamics. Fig. 5a,b show the time- and wavelength-resolved streak images and the decay time constants at 15 K for the core-shell SQW and the core-shell MQWs respectively. The decay time constants were simply obtained by measuring the time corresponding to a reduction of the PL intensity by a factor 1/e at each wavelength. In Fig. 5a, the core-shell InGaN SQW shows a remarkably fast recombination time about 100 ps. Nitride materials itself have a high oscillator strength due to the small Bohr radius compared to narrow bandgap III-V semiconductors.[40, 41] However, the strong polarization fields in QWs separate the electron and hole wavefunctions and reduce the oscillator strength, which is inversely proportional to the radiative recombination time. In the case of the core-shell InGaN QWs, the polarization fields are reduced due to the strain relaxation in the vertical nanostructures and the small polarization discontinuities in the semipolar facets.[20, 42] In the core-shell MQWs in Fig. 5b, although the thick QWs have a little bit longer recombination time than the thin QWs, they also show fast recombination times. This is a noticeable result and indicates again an ignorable QCSE in the core-shell nanostructures. In the case of conventional InGaN QWs grown on planar substrates, the QCSE rapidly increases with the In contents and the thickness of QWs (Fig. S5†).[43] In the time evolutions of PL emission, the core-shell QWs do not show a distinctive spectral shift behavior with decay (Fig. 5a,b). The high energy peak of the core-shell SQW at 3.27 eV shown after fast decay (Fig. 5a) is attributed to the donor acceptor pair emission of GaN. In the case of the core-shell MQW, although the second and the third peaks from the thick InGaN QWs show a relatively longer decay compared to the first, thinnest QW, each peaks do not show a peak shift with time. This is in contrast to the planar QWs, having a large red shift in their PL spectrum with time (Fig. S5†). Many possibilities can be concerned for this spectral shift phenomenon in InGaN QWs. Generally, InGaN QWs possess a large potential fluctuation induced by the local variation of In composition and well thickness. Therefore, a carrier transport can occur during the recombination from the higher energy to the lower energy, resulting in a fast (slow) decay in the high (low) energy side of QW emission.[44] However, both the core-shell and planar QW groups have potential fluctuations by the inhomogeneous well width and In composition, which means that carrier transport cannot be a sufficient reason for the spectral shift phenomenon in the planar InGaN QW. Another explanation is related to the built-in electric field. The QCSE becomes severe at a low energy side since the low energy side represents a large In content and a wide well width.[45, 46] We already show the strong wavelength dependence of the recombination time in Fig. 5c. Besides, the QCSE of QWs can vary
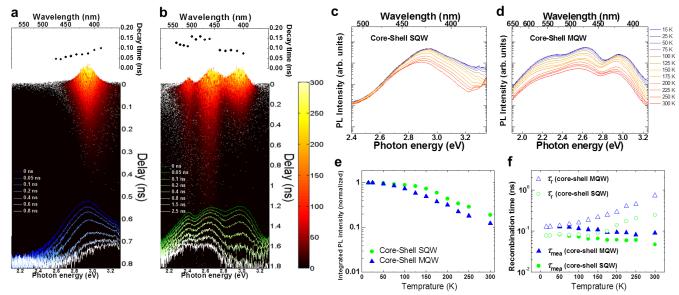

Fig. 5 (a,b) Streak images at 15 K for (a) the core-shell InGaN SQW and (b) the core-shell InGaN MQWs. Decay time constants at different wavelength and time evolution of PL emission (log-scale) after pulse excitation are also shown above and below streak images, respectively. (c,d) Temperature dependent PL spectrum for (c) the core-shell SQW and (d) the core-shell MQWs. (e,f) Comparison of (e) integrated PL intensity and (f) measured recombination time constants as a function of temperature for the core-shell SQW (green circles) and the core-shell MQWs (blue triangles). Calculated radiative recombination nanoconstants are also plotted in (f) for the core-shell SQW (green open circles) and the core-shell MQWs (blue open triangles)

with time due to the change of carrier density. At the initial stage of the pulse excitation, the photo-generated large number of carriers screens the QCSE, resulting in blue shift, and the screen effect is reduced with decay time by the carrier recombination (red shift). These mixed effects induce complex radiative recombination behaviors and red shift the planar QW emission with time. We also observed a peak shift in the planar QWs in the excitation power dependent experiment, but no change in the core-shell QWs. Therefore, we can conclude that the built-in electric field plays an important role in the transition energy and the recombination dynamics of InGaN QWs, and the core-shell nanostructures have a negligible built-in electric field and high oscillator strength in the broad spectral range, which are difficult to achieve in planar QWs.

Temperature dependent optical properties of GaN/InGaN core-shell nanostructures

Finally, we confirmed the temperature dependence of the PL intensity and the recombination time in order to estimate the internal quantum efficiency (IQE) and extract the radiative recombination time. Fig. 5c,d show the temperature dependent PL spectrum (log scale) from 15 K to 300 K for the core-shell SQWs and the core-shell MQWs, respectively, and we plot the integrated PL intensity of both samples as a function of temperature in Fig. 5e. The ratio of PL intensity between the low temperature (15 K) to each temperature (T) is related to the IQE [$\eta(T)$] of samples. The core-shell InGaN QWs show IQEs around 10 ~ 20 %. The core-shell QWs are not grown at the optimized conditions and thus the IQE can be improved further. However, there is an important fact that the core-shell QWs have uniform IQE within a broad spectrum range. This result is related to uniform oscillator strength for the core-shell InGaN QWs in Fig. 5b. Therefore, the core-shell InGaN QWs can have high quantum efficiency even with high In contents and thick QW thickness.

Next, we compared the measured recombination times of the integrated QW emission with temperature in Fig. 5f, and it shows temperature-insensitive recombination time. We also plot the radiative recombination time as a function of temperature. The radiative recombination time (τ_r) has a relationship with the IQE (η) and measured recombination time (τ_{mea}) as the following: $\tau_r = \tau_{mea}/\eta$. Therefore, it can be extracted from Fig. 5e and 5f with the assumption of $\eta \sim 1$ at the lowest temperature. In semiconductors, the radiative recombination time increases with temperature due to the spreading of the carrier distribution into the density of states.[47] The radiative recombination times of InGaN QWs are almost constant below 100 K and then increase with temperature above 100 K. This is related to the quantum dot-like localized exciton property[48] at low temperature and the two dimensional QW property[47] at high temperature. Even at room temperature, the core-shell QW samples show sub-ns fast radiative recombination time due to the minimized built-in electric field.

Experimental section

Sample fabrication

To form GaN nanostructure templates, we prepared 2 μm-thick Ga-polar GaN films grown on 2-inch sapphire (0001) substrates using MOCVD, and exposed the wafers to 1000 sccm HCl gas at a high temperature of 1000 °C. In this CVE process, hot HCl gas decomposes GaN into GaCl. N_2 gas was flowed as a carrier gas and NH_3 was also used to control the etching speed. Generally, 5 min etching forms 1 μm-long GaN nanostructures in a whole wafer

uniformly. The pressure of the etching chamber was set at atmospheric pressure. During the MOCVD regrowth process, all InGaN QWs and GaN barriers were grown at 680 °C and at 850 °C, respectively, and other growth parameters for InGaN QWs were as follows: P = 350 Torr, NH_3= 10000 sccm, TMGa = 5 sccm, TMIn = 300 sccm.

Structural and optical characterization

We used SEM (Hitachi-S4800) and spherical aberration-corrected S/TEM (JEOL-ARM200F, 200 kV acceleration voltage) to observe the nanostructure and QW images. The cross-sectional TEM samples were prepared by mechanically polishing with an ion-milling process (Gatan PIPS691) or focused ion beam milling (FEI Helios nanolab). The In composition of InGaN QWs was analyzed by using EDS (Bruker, Qauntax 400), installed in TEM. For both the time-integrated PL and time-resolved PL measurements, the samples were mounted in a closed-cycle cryostat that maintains stable temperatures from 10 to 300 K. A continuous-wave 325 nm He-Cd laser and a high sensitive photomultiplier tube detector were used for time-integrated PL. A 340 nm frequency-doubled, mode-locked (200 fs) Ti:Sapphire laser and a streak camera system were used to obtain the time-resolved PL spectra. The FWHM of the instrument response function of this system is less than 50 ps. Monochromatic CL images (Gatan, mono4) were acquired at room temperature with an acceleration voltage of 5 kV.

Conclusions

In the present work, we demonstrated the broadband visible-light emitting GaN/InGaN core-shell quantum nanostructures, which were formed on non-polar and semi-polar multi-facets by a dislocation-eliminating CVE technique followed by MOCVD. From many points of view, the core-shell InGaN QWs show lots of distinctive advantages compared to the planar InGaN QWs. The CVE process eliminates dislocations in the nanostructures and forms the high crystal quality GaN nanostructure. The introduction of various thicknesses of quantum wells and the multi-facets of the core-shell nanostructures enables a broad spectrum of the entire visible range, even with the single InGaN growth temperature. Together with improved light extraction, the core-shell nanostructures show a high quantum efficiency in a long wavelength region even at room temperature due to their high crystal quality and negligible quantum confined Stark effect. The minimized polarization fields in the core-shell nanostructures induce ultrafast radiative recombination time less than 200 ps in a broad spectral range, which is difficult to achieve in the conventional InGaN quantum wells.

Although our self-formed core-shell nanostructures have a variation in size and a random position compared to the pattering growth method, the CVE method forms high density, dislocation-eliminated core-shell nanostructures on a wafer level without patterning process. Therefore, our approach suggests the practical and favorable method to form dislocation- and polarization field-eliminated core-shell nanostructures, and it may serve as a promising platform for highly efficient phosphor-free white LEDs.

Notes and references

Department of Physics, KI for the NanoCentury, KAIST, Daejeon, 305-701, Republic of Korea. E-mail: yhc@kaist.ac.kr; Tel:+82 42 350 2549

References

1   J. Y. Tsao, *IEEE Circuits Devices Mag.* 2004, **20**, 28.

2   E. F. Schubert, J. K. Kim, *Science* 2005, **308**, 1274.

3   M. R. Krames, O. B. Shchekin, R. Mueller-Mach, G. O. Mueller, Z. Ling, G. Harbers, M. G. Craford, *J. Display Technol.* 2007, **3**, 160.

4   S. Pimputkar, J. S. Speck, S. P. DenBaars, S. Nakamura, *Nat Photon* 2009, **3**, 180.

5   M. H. Crawford, *IEEE J. Sel. Top. Quantum Electron.* 2009, **15**, 1028.

6   T. Takeuchi, S. Sota, M. Katsuragawa, M. Komori, H. Takeuchi, H. Amano, I. Akasaki, *Jpn. J. Appl. Phys* 1997, **36**, L382.

7   P. M. F. J. Costa, R. Datta, M. J. Kappers, M. E. Vickers, C. J. Humphreys, D. M. Graham, P. Dawson, M. J. Godfrey, E. J. Thrush, J. T. Mullins, *Phys. Status Solidi A* 2006, **203**, 1729.

8   M.-H. Kim, M. F. Schubert, Q. Dai, J. K. Kim, E. F. Schubert, J. Piprek, Y. Park, *Appl. Phys. Lett.* 2007, **91**, 183507.

9   Y.-L. Li, Y.-R. Huang, Y.-H. Lai, *Appl. Phys. Lett.* 2007, **91**, 181113.

10   M. Boroditsky, T. F. Krauss, R. Coccioli, R. Vrijen, R. Bhat, E. Yablonovitch, *Appl. Phys. Lett.* 1999, **75**, 1036.

11   H. Gao, F. Yan, Y. Zhang, J. Li, Y. Zeng, G. Wang, *J. Appl. Phys.* 2008, **103**, 014314.

12   I. Schnitzer, E. Yablonovitch, C. Caneau, T. J. Gmitter, A. Scherer, *Appl. Phys. Lett.* 1993, **63**, 2174.

13   D. S. Wuu, W. K. Wang, K. S. Wen, S. C. Huang, S. H. Lin, S. Y. Huang, C. F. Lin, R. H. Horng, *Appl. Phys. Lett.* 2006, **89**, 161105.

14   D. Xiao, K. W. Kim, S. M. Bedair, J. M. Zavada, *Appl. Phys. Lett.* 2004, **84**, 672.

15   S.-H. Park, D. Ahn, *Appl. Phys. Lett.* 2007, **90**, 013505.

16   C. Kölper, M. Sabathil, F. Römer, M. Mandl, M. Strassburg, B. Witzigmann, *Phys. Status Solidi A* 2012, **209**, 2304.

17   Y. J. Hong, C.-H. Lee, A. Yoon, M. Kim, H.-K. Seong, H. J. Chung, C. Sone, Y. J. Park, G.-C. Yi, *Adv. Mater.* 2011, **23**, 3284.

18   H.-S. Chen, Y.-F. Yao, C.-H. Liao, C.-G. Tu, C.-Y. Su, W.-M. Chang, Y.-W. Kiang, C. C. Yang, *Opt. Lett.* 2013, **38**, 3370.

19   J. R. Riley, S. Padalkar, Q. Li, P. Lu, D. D. Koleske, J. J. Wierer, G. T. Wang, L. J. Lauhon, *Nano Lett.* 2013, **13**, 4317.

20   S.-H. Park, *J. Appl. Phys.* 2002, **91**, 9904.

21   H. P. T. Nguyen, S. Zhang, K. Cui, X. Han, S. Fathololoumi, M. Couillard, G. A. Botton, Z. Mi, *Nano Lett.* 2011, **11**, 1919.

22   W. Guo, M. Zhang, A. Banerjee, P. Bhattacharya, *Nano Lett.* 2010, **10**, 3355.

23   J. P. Ahl, H. Behmenburg, C. Giesen, I. Regolin, W. Prost, F. J. Tegude, G. Z. Radnoczi, B. Pécz, H. Kalisch, R. H. Jansen, M. Heuken, *Phys. Status Solidi C* 2011, **8**, 2315.

24   S. D. Hersee, X. Sun, X. Wang, *Nano Lett.* 2006, **6**, 1808.

25   R. Koester, J.-S. Hwang, D. Salomon, X. Chen, C. Bougerol, J.-P. Barnes, D. L. S. Dang, L. Rigutti, A. de Luna Bugallo, G. Jacopin, M. Tchernycheva, C. Durand, J. Eymery, *Nano Lett.* 2011, **11**, 4839.

26   C. Tessarek, M. Bashouti, M. Heilmann, C. Dieker, I. Knoke, E. Spiecker, S. Christiansen, *J. Appl. Phys.* 2013, **114**, 144304.

27   S.-M. Ko, J.-H. Kim, Y.-H. Ko, Y. H. Chang, Y.-H. Kim, J. Yoon, J. Y. Lee, Y.-H. Cho, *Cryst. Growth Des.* 2012, **12**, 3838.

28   Y. B. Hahn, R. J. Choi, J. H. Hong, H. J. Park, C. S. Choi, H. J. Lee, *J. Appl. Phys.* 2002, **92**, 1189.

29   C. B. Vartuli, S. J. Pearton, C. R. Abernathy, J. D. MacKenzie, F. Ren, J. C. Zolper, R. J. Shul, *Solid-State Electron.* 1997, **41**, 1947.

30   J.-H. Kim, C.-S. Oh, Y.-H. Ko, S.-M. Ko, K.-Y. Park, M. Jeong, J. Y. Lee, Y.-H. Cho, *Cryst. Growth Des.* 2012, **12**, 1292.

31   D. Holec, P. Costa, M. Kappers, C. Humphreys, *J. Cryst. Growth* 2007, **303**, 314.

32   B. Leung, Q. Sun, C. D. Yerino, J. Han, M. E. Coltrin, *Semicond. Sci. Technol.* 2012, **27**, 024005.

33   X. Zhang, P. D. Dapkus, D. H. Rich, I. Kim, J. T. Kobayashi, N. P. Kobayashi, *J. Electron. Mater.* 2000, **29**, 10.

34   Y. Sakata, Y. Inomoto, K. Komatsu, *J. Cryst. Growth* 2000, **208**, 130.

35   B. Deveaud, F. Clérot, N. Roy, K. Satzke, B. Sermage, D. S. Katzer, *Physical Review Letters* 1991, **67**, 2355.

36   J.-H. Kim, Y.-H. Ko, S.-H. Gong, S.-M. Ko, Y.-H. Cho, *Sci. Rep.* 2013, **3**, 2150.

37   T. K. Sharma, E. Towe, *J. Appl. Phys.* 2009, **106**, 104509.

38   M. Hao, H. Ishikawa, T. Egawa, C. L. Shao, T. Jimbo, *Appl. Phys. Lett.* 2003, **82**, 4702.

39   I. Shalish, L. Kronik, G. Segal, Y. Rosenwaks, Y. Shapira, U. Tisch, J. Salzman, *Phys. Rev. B* 1999, **59**, 9748.

40   S. Faure, T. Guillet, P. Lefebvre, T. Bretagnon, B. Gil, *Phys. Rev. B* 2008, **78**, 235323.

41   G. Christmann, R. Butté, E. Feltin, J. F. Carlin, N. Grandjean, *Phys. Rev. B* 2006, **73**, 153305.

42   Z. Liang, I. H. Wildeson, R. Colby, D. A. Ewoldt, T. Zhang, T. D. Sands, E. A. Stach, B. Benes, R. E. García, *Nano Lett.* 2011, **11**, 4515.

43   S. F. Chichibu, A. C. Abare, M. P. Mack, M. S. Minsky, T. Deguchi, D. Cohen, P. Kozodoy, S. B. Fleischer, S. Keller, J. S. Speck, J. E. Bowers, E. Hu, U. K. Mishra, L. A. Coldren, S. P. DenBaars, K. Wada, T. Sota, S. Nakamura, *Mater. Sci. Eng., B* 1999, **59**, 298.

44   S.-W. Feng, Y.-C. Cheng, Y.-Y. Chung, C. C. Yang, Y.-S. Lin, C. Hsu, K.-J. Ma, J.-I. Chyi, *J. Appl. Phys.* 2002, **92**, 4441.

45   J.-H. Kim, D. Elmaghraoui, M. Leroux, M. Korytov, P. Vennéguès, S. Jaziri, J. Brault, Y.-H. Cho, *Nanotechnology* 2014, **25**, 305703.

46   S. F. Chichibu, T. Azuhata, T. Sota, T. Mukai, S. Nakamura, *J. Appl. Phys.* 2000, **88**, 5153.

47   L. C. Andreani, F. Tassone, F. Bassani, *Solid State Commun.* 1991, **77**, 641.

48   G. Wang, S. Fafard, D. Leonard, J. E. Bowers, J. L. Merz, P. M. Petroff, *Appl. Phys. Lett.* 1994, **64**, 2815.

Nanoscale Accepted Manuscript